Upgrades to the Artemis Material Science Station

Contact *yu.zhang@stfc.ac.uk*

Y. Zhang, C. Toolan, R. T. Chapman, A. S. Wyatt, C. Sanders and E. Springate

Central Laser Facility, STFC Rutherford Appleton Laboratory, Harwell Campus, Didcot OX11 0QX

Introduction

The material science station at Artemis is a dedicated facility for the study of transient phenomena on surfaces. Pioneering work done at this end station on topics such as electron dynamics in graphene [1,2], correlated ground states [3,4], and spin- and valley-physics [5] has helped promote a whole field of research on ultrafast phenomena in two-dimensional (2D) and layered materials. However, with the development of pump-probe photoemission as a technique to explore ultrafast phenomena, new experimental challenges have become critical, such as the need to manage the space charge effect [6], in which Coulombic interaction of photoelectrons degrades energy and angular resolution. Meanwhile, at the same time that pump-probe photoemission techniques have been developing into a mature and well-established research field, the research community is also becoming increasingly interested in reducing the photoemission probing area (*i.e.*, the beam-spot size) [7,8], in order to be able to make spatially-resolved measurements of inhomogeneous samples—for example, for the study of individual crystalline domains in multidomain samples.

Artemis has recently upgraded its laser system to a new 100-kHz optical parametric chirped pulse amplifier (OPCPA) laser, and a new material science beamline is being built to generate an extreme-ultraviolet (XUV) probe by high-harmonic generation via an Ar gas jet. By increasing our repetition rate, we expect to reduce space-charge limitations, since the number of photons per pulse can now be reduced without sacrificing total photons per second. Furthermore, by reducing the number of photons per pulse, we can reduce the size of the beam-spot without increasing space-charge [6]. One of the aims of the new beamline is to offer the option of a small XUV beam-spot with a diameter on the scale of tens of μm (contrasting with hundreds of μm in Artemis's original 1-kHz setup). This will open the door to spatially-dependent studies of small single-domains.

In order to take advantage of this new capability, we have made two major upgrades to the material science station in 2019. First, we have motorized the commercial sample manipulator. Second, we have installed a new commercial 2D photoelectron detector that will enable efficient low-noise data collection at even low count rates such as those that can be expected for low-flux, small-spot-size measurements.

Motorization of sample manipulator

The sample manipulator in the material science station is a five-axis manipulator allowing movement in three perpendicular translation directions (X, Y and Z), polar rotation about the vertical axis (θ), and in-plane (azimuthal) rotation of sample (φ). The upgrade that we report here is the motorization of the X, Y, Z and θ motions of the manipulator (Fig. 1). This was implemented as a commercial solution by the company VAb. Repeatability in the three translation directions is 0.01 mm, and is 0.001° in the θ rotation direction. The motors are controlled remotely, either by a joystick or by a computer running Labview-based control software. We intend to integrate the sample motion control into our existing Labview-based data acquisition and control system. This will permit spatially dependent scanning of sample domains on the scale of tens of μm, consistent with the capabilities of the new beamline to deliver spot sizes on this order.

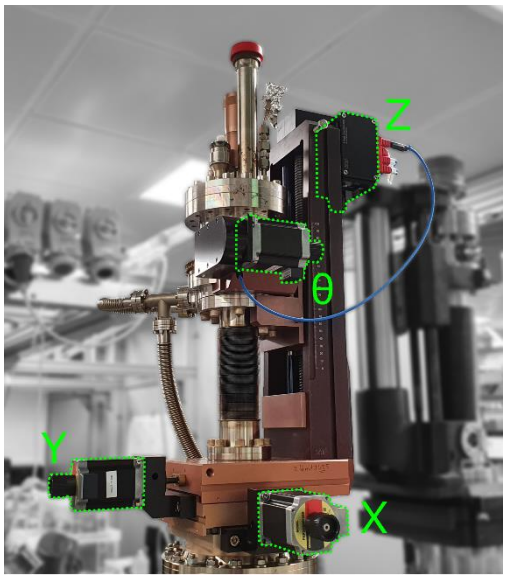

Figure 1. Photograph of the manipulator on the motorized translation stage. Driving motors are highlighted in green.

2D photoelectron detector

The Artemis material science station uses a SPECS Phoibos 100 hemispherical analyzer, together with a 2D detector package (microchannel plate (MCP) detector, phosphor screen, camera, and graphics processing unit), to identify the emission angle and kinetic energy of electrons photoemitted from a sample. Good detector performance is critical for efficient spectroscopy measurements. Until recently, we have used a detector package based on a charge-coupled-device (CCD) camera, which directly images the fluorescence on the phosphor screen that occurs when impinging photoelectrons, having passed between the hemispheres of the analyzer, induce electron cascades in the MCP. The spectral data have then been obtained by integrating over long exposure times or by summing accumulated images.

As an alternative approach, if the camera speed is sufficiently high relative to the rate at which photoelectrons impinge on the detector, the acquisition computer can identify spots on the phosphor screen one by one and thus identfy the impinging of individual photoelectrons. The computer then registers the positions of each spot ("pulse") in a digital image. This approach is called "pulse-counting mode." It eliminates a great deal of background noise; furthermore, the intrinsically complex dependency on screen voltage (and other variables) of spot brightness does not greatly affect the pulse-counting detection process. Thus, data quality can in many cases be improved relative to summing- or integrating-based imaging approaches, especially when the total counts are low, as is often the case in pump-probe measurements.

However, it is important to acknowledge that, for high count rates relative to the camera speed, closely-spaced fluorescence spots

start to coalesce, and the conjoined spots from multiple incident electrons may be incorrectly interpreted by pulse-counting algorithms as being due to a single electron; thus, pulse-counting mode fails at very high count rates. A key metric of detector performance is "dynamic range," defined as the range in which the relationship between rate of electron incidence on the detector is linear with respect to the measured count rate. For pulse-counting methods, this relationship becomes nonlinear at high count rates.

The new detector package (from SPECS GmbH) achieves a large dynamic range in pulse-counting mode by using a fast camera (Flir Grasshopper 3, GS3-U3-23S6M, 163 frames per second) based on complementary metal-oxide semiconductor (CMOS) technology. The detector's working principle is illustrated in Fig. 2. Because of the speed of the fast CMOS camera, no more than a few spots are counted in a single image up to even very high count rates. Meanwhile, the fast data collection rate of the camera is coupled with fast data processing via parallel calculation in the graphics processing unit. Quick searching and recognition of electron pulses in an image can be finished in a few milliseconds, which is necessary for the fast frame-rate of the camera. As a result of this increased image rate and computing power, the 2D-CMOS detector features a large range of linear response—specified by the manufacturer from 5 to 6e6 counts per second—and a decreased dark-count intensity.

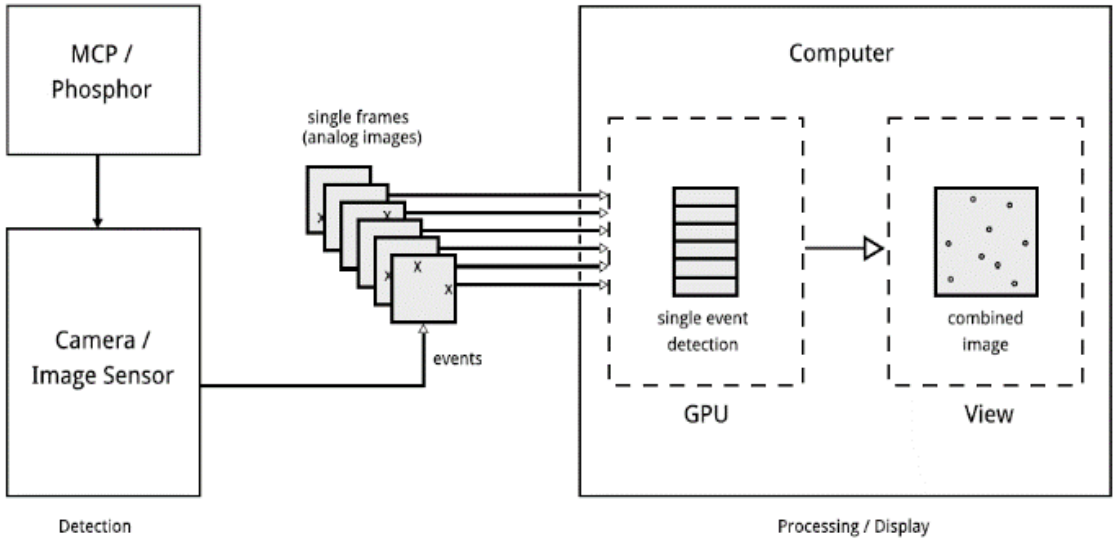

Figure 2. Pulse-counting method for the 2D-CMOS detector [SPECS Prodigy software package].

References

1. J. C. Johannsen, S. Ulstrup, F. Cilento, A. Crepaldi, M. Zacchigna, C. Cacho, I. C. E. Turcu, E. Springate, F. Fromm, C. Raidel, T. Seyller, F. Parmigiani, M. Grioni, and P. Hofmann, Phys. Rev. Lett. **111** 027403 (2013).
2. I. Gierz, J. C. Petersen, M. Mitrano, C. Cacho, E. Turcu, E. Springate, A., Stohr, Al Kohler, U. Starke, and A. Cavalleri, Nat. Mat. **12** 1119 (2013).
3. J. C. Petersen, S. Kaiser, N. Dean, A. Simoncig, H. Y. Liu, A. L. Cavalieri, C. Cacho, I. C. E. Turcu, E. Springate, F. Frassetto, L. Poletto, S. S. Dhesi, H. Berger, and A. Cavalleri, Phys. Rev. Lett. **107** 177402 (2011).
4. C. Monney, M. Puppin, C. W. Nicholson, M. Hoesch, R. T. Chapman, E. Springate, H. Berger, A. Magrez, C. Cacho, R. Ernstorfer, M. Wolf, Phys. Rev. B **94** 165165 (2016).
5. S. Ulstrup, A. Grubišić Čabo, D. Biswas, J. M. Riley, M. Dendzik, C. E. Sanders, M. Bianchi, C. Cacho, D. Matselyukh, R. T. Chapman, E. Springate, P. D. C. King, J. A. Miwa, P. Hofmann, Phys. Rev. B **95** 041405 (2017).
6. S. Hellman, K. Rossnagel, M. Marczynski-Bühlow, and L. Kipp, Phys. Rev. B **79** 035402 (2009).
7. E. Rotenberg and A. Bostwick, J. Synchrotron Rad. **21** 1048 (2014).
8. M. Hoesch, T. K. Kim, P. Dudin, H. Wang, S. Scott, P. Harris, S. Patel, M. Matthews, D. Hawkins, S. G. Alcock, T. Richter, J. J. Mudd, M. Basham, L. Pratt, P. Leicester, E. C. Longhi, A. Tamai, and F. Baumberger, Rev. Sci. Instrum. **88** 013106 (2017).